The Evolving Role of Materials in Implantable Antenna Design: A Comprehensive Review

Sumer Singh Singhwal, Ladislau Matekovits, and Ildiko Peter

This article presents a comprehensive review of implantable antenna technology with a primary focus on the role of materials in shaping electromagnetic performance, biostability, and clinical viability. Core substrate classes—including polytetrafluoroethylene (PTFE)–ceramic laminates, flexible polyimide and liquid crystal-polymer (LCP) films, and bioceramics such as alumina and zirconia—are discussed in terms of miniaturization, loss, manufacturability, and interaction with biological tissues. Encapsulation and coating materials are examined for their influence on resonance stability, specific absorption rate (SAR), and long-term reliability, while conductive and ground materials are reviewed with respect to chemical durability and current distribution. Magnetic and metamaterial (MTM)-enhanced layers are assessed as material-driven approaches for bandwidth enhancement, polarization control, and electrically small antenna design under strong tissue loading. Emerging directions include low-loss rutile TiO_2, perovskite microwave ceramics, low-temperature co-fired ceramic (LTCC) platforms, biodegradable polymers, and dielectric resonator antenna (DRA) architectures, which collectively enable reduced RF heating and improved clinical compatibility.

Digital Object Identifier 10.1109/MAP.2026.3721821
Date of current version: 9 October 2026

EDITOR'S NOTE



Asimina Kiourti

Wireless implants are transforming health care, enabling continuous physiological monitoring, closed-loop therapies, and wireless power transfer for numerous clinical applications. However, designing implantable antennas for the lossy and dispersive biological tissue environment is highly challenging. This article tackles these challenges through a material-centric review of implantable antennas over the past decade. The review carefully examines how substrate selection, encapsulation strategies, and emerging material platforms drive miniaturization, biocompatibility, radiation performance, safety, and clinical translation.

The "Bioelectromagnetics" column welcomes articles on biomedical applications of electromagnetics, antennas, and propagation in terms of research, education, outreach, and more. If you are interested in contributing, please e-mail me at kiourti.1@osu.edu.

By integrating material properties with antenna structures and biocompatibility constraints, this review provides a unified perspective on material-centric strategies for next-generation implantable antennas across established and emerging biomedical frequency bands.

INTRODUCTION

Implantable medical devices (IMDs) are electronic systems surgically placed inside the human body to perform long-term diagnostic, therapeutic, monitoring, or assistive functions. Their clinical relevance continues to grow; the global IMD market was valued at US$92.9 billion in 2024 and is projected to exceed US$148 billion by 2031, driven by cardiovascular, neurological, orthopedic, ophthalmic, and ingestible technologies [1]. Wireless biotelemetry enabled by implantable antennas is central to this growth, supporting continuous physiological monitoring, closed-loop therapy, and emerging wireless power transfer paradigms. Figure 1 shows a conceptual illustration of an implantable antenna embedded within various biological tissue layers.

Modern IMDs integrate sensors, electronics, power sources, and a miniature antenna within a severely constrained volume. Unlike free-space antennas, implantable antennas operate inside a highly lossy, dispersive, and electrically dense medium. Biological tissues exhibit relative permittivity often exceeding 30 and conductivity approaching 1–2 S/m, leading to shortened

This work is licensed under a Creative Commons Attribution 4.0 License.
For more information, see https://creativecommons.org/licenses/by/4.0/

wavelengths, reduced radiation efficiency, strong near-field confinement, and increased risk of localized heating. Under these conditions, antenna geometry alone cannot guarantee stable performance. Instead, the material stack—substrate, metallization, encapsulation, and surrounding tissue—largely determines the impedance stability, efficiency, SAR, and long-term reliability.

Over the past two decades, implantable antennas have been extensively reviewed from system-level, architectural, and application-driven perspectives [2], [3], [4], [5], [6], [7], [8], [9], [10]. These works established foundational design principles, regulatory constraints, and clinical use cases. However, despite rapid progress in materials science and biomedical manufacturing, no recent review has focused explicitly on materials as the primary design driver, particularly for developments over the last decade. This gap is increasingly relevant as implantable antennas transition from laboratory prototypes toward clinically viable and chronically implanted systems.

Material innovation has been a dominant force in this transition. High-permittivity PTFE–ceramic laminates (e.g., RO3010, RO3210, and RO6010) enabled aggressive miniaturization in the Medical Implant Communication Service (MICS) and industrial, scientific, and medical (ISM) bands; flexible polyimide and LCP films supported conformal and injectable geometries; bioceramics such as alumina and zirconia improved long-term encapsulation and resonance stability; and soft polymers, including polydimethylsiloxane (PDMS) and medical-grade silicones, became essential for SAR control and mechanical compliance. More recently, magneto–dielectric loading, metamaterial-inspired substrates, and 3D-printed biocompatible polymers have introduced new degrees of freedom for bandwidth enhancement, polarization control, and volumetric antenna architectures.

This review adopts a material-centric perspective on implantable antenna design over the last decade. Rather than cataloging geometries, it examines how substrate permittivity and loss, encapsulation strategies, conductive and ground materials, and emerging composites shape electromagnetic behavior under severe tissue loading and clinical constraints. It also highlights material-driven bottlenecks to translation and promising platforms—such as LTCC, perovskite ceramics, rutile TiO_2, and hybrid polymer–ceramic stacks—for next-generation implantable wireless systems. Figure 2 shows representative contemporary prototypes of implantable antennas.

ELECTROMAGNETIC DESIGN CONSTRAINTS IN BIOLOGICAL MEDIA

Implantable antennas operate inside a complex electromagnetic environment formed by multilayer biological tissues that are inherently lossy, dispersive, and strongly frequency dependent. At the operational frequencies of medical implants—spanning the MICS, Medical Device Radiocommunication Service (MedRadio), ISM, and emerging ultra-wideband (UWB) bands summarized in Tables 1 and 2—soft tissues such as skin, muscle, fat, blood, and bone exhibit high relative permittivity and nonnegligible conductivity. The resulting shortened wavelengths, strong attenuation, and nonuniform near-field distributions fundamentally alter radiation mechanisms compared with free space and impose strict constraints on antenna efficiency, bandwidth, and safety.

According to the widely adopted Gabriel tissue models [15], the relative permittivity (ε_r) and conductivity (σ) of biological tissues vary significantly across frequency, as summarized in Table 3. For implantable antennas, this environment effectively acts as a high-permittivity and lossy loading medium that continuously perturbs impedance and resonance. Consequently, the antenna material stack must function as an impedance transformer between the high-ε_r tissue and the low-ε_r external environment. Substrates with moderate to high permittivity (typically $\varepsilon_r \approx 8-11$), such as PTFE–ceramic laminates, are therefore widely employed to reduce physical size while maintaining manageable impedance matching under tissue loading.

Encapsulation layers play an equally critical role in shaping electromagnetic behavior. Low-permittivity polymers such as PDMS and medical-grade silicone ($\varepsilon_r \approx 2.7-3.0$) soften the abrupt dielectric transition at the tissue boundary, reducing reflection losses and moderating near-field absorption. In contrast, poorly

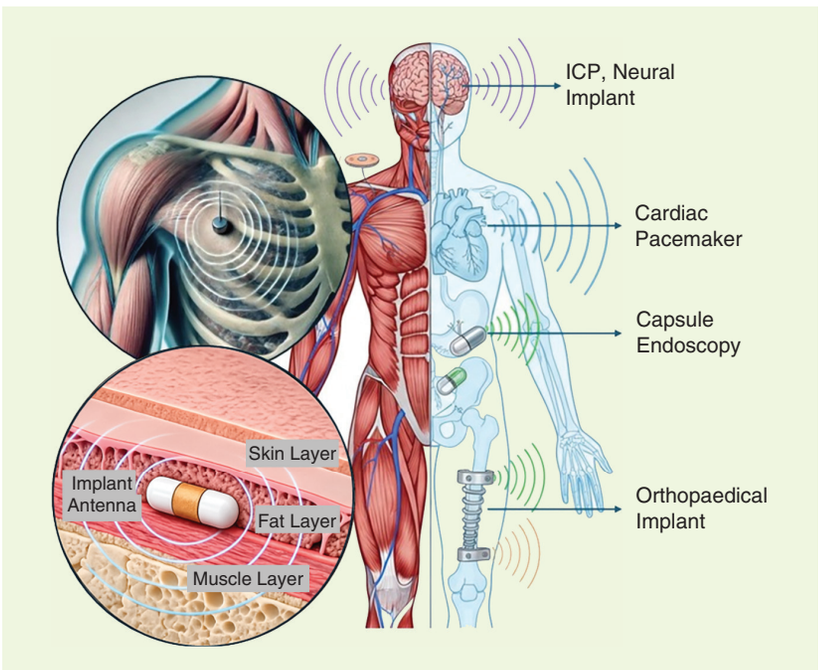


FIGURE 1. A conceptual illustration of IMDs. ICP: intracranial pressure.

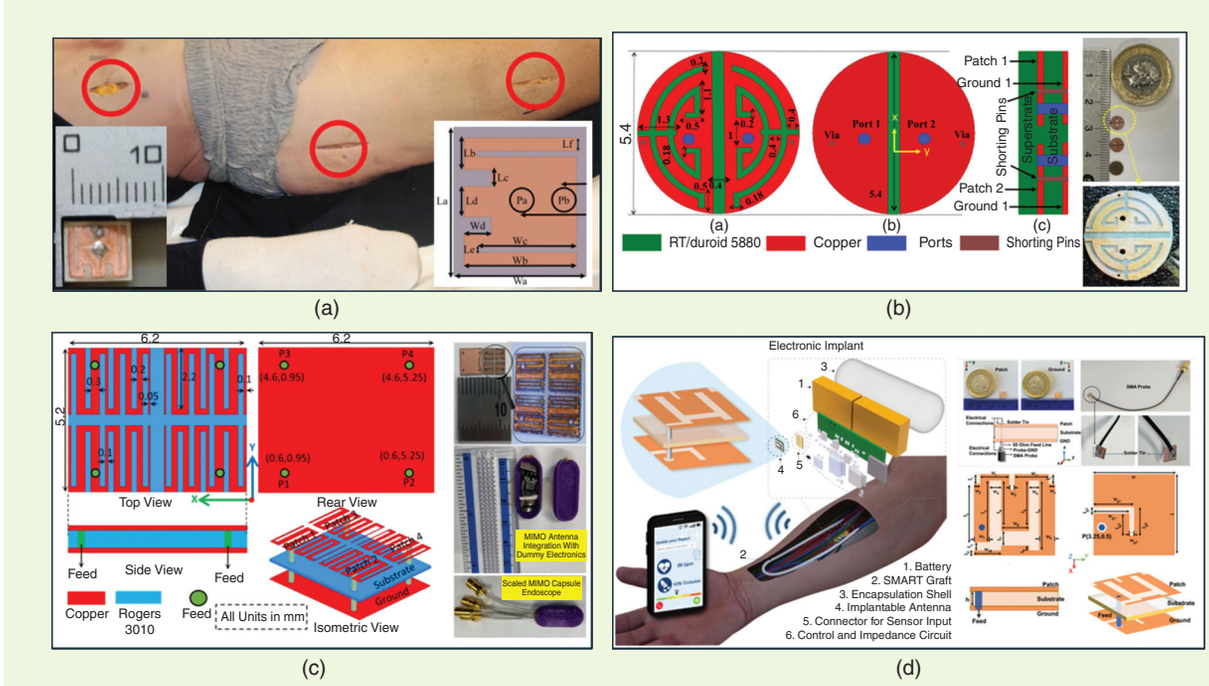


FIGURE 2. Representative contemporary implantable antenna implementations. (a) Miniature 2.4/4.8 GHz implantable antenna validated in a postmortem human subject [34]. (b) Compact in-band full-duplex antenna for deeply implantable biomedical Internet of Things applications [52]. (c) Miniaturized four-port MIMO antenna for high-data-rate wireless capsule endoscopy [53]. (d) Compact dual-band implantable antenna for wireless biotelemetry in arteriovenous grafts [71]. GND: ground; SMA: subMiniature version A.

TABLE 1. ISM FREQUENCY BANDS [11], [12].

ISM Band	Frequency Range/Tolerance	Representative Implantable Applications
6.78 MHz	±15 kHz	Near-field inductive/resonant WPT for deep implants and biosensors
13.56 MHz	±7 kHz	RFID-based implants, magnetic coupling, and short-range powering links
27.12 MHz	±163 kHz	Tissue-phantom testing, low-frequency characterization, and dielectric heating studies
40.68 MHz	±20 kHz	Experimental magnetic-resonant coupling and inductive powering testbeds
433.92 MHz	433.05–434.79 MHz	Short-range implant–relay communication and capsule/dental telemetry
915 MHz	902–928 MHz (±13 MHz)	Sub-GHz implant telemetry, WPT, pacemaker links, and capsule/vascular monitoring
2.45 GHz	2,400–2,500 MHz (±50 MHz)	Dominant ISM telemetry band for cardiac, neural, capsule, oral, and MIMO implants
5.8 GHz	5,725–5,875 MHz (±75 MHz)	High-data-rate short-range telemetry, MIMO implants, and UWB-related links
24.125 GHz	24–24.25 GHz (±125 MHz)	Prospective mmWave implant sensing, localization, and shallow-tissue telemetry
61.25 GHz	61–61.5 GHz (±250 MHz)	Future short-range mmWave powering, localization, and epidermal/neural links
122.5 GHz	122–123 GHz (±500 MHz)	Prospective sub-THz microscale implant communication
245 GHz	244–246 GHz (±1 GHz)	Future THz intra-body sensing, imaging, and smart biointegrated systems

matched or overly thin encapsulation can lead to strong electric-field concentration at the tissue interface, increasing impedance instability and localized heating. For this reason, encapsulant thickness—typically in the range of 100 μm to 1 mm—must be carefully co-optimized with substrate properties and operating frequency. SAR is a central safety metric for implantable antennas, quantifying the rate at which electromagnetic energy is absorbed by tissue. SAR depends on the local electric-field strength, tissue conductivity, and mass density and becomes particularly critical for deeply implanted radiators operating in high-loss media [2], [3], [4], [5], [6]. Even modest mismatches in permittivity between the antenna, encapsulation, and tissue can produce localized field enhancement and SAR hotspots. IEEE and ICNIRP standards therefore impose strict limits on localized and whole-body SAR to prevent harmful temperature rise, as summarized in Table 4. Material selection directly influences SAR behavior. High-ε_r substrates confine fields within the antenna structure, limiting leakage into surrounding tissue, whereas low-ε_r encapsulants distribute fields more evenly and reduce peak SAR. Bioceramic coatings such as alumina or glass further stabilize the dielectric interface, restrict ionic conduction, and improve long-term electrical stability. Conversely, exposed metallic surfaces or highly conductive substrates in direct contact with tissue can lead to excessive capacitive coupling, impedance detuning, and SAR violations.

Loss tangent constitutes an additional key constraint. In an environment where tissue attenuation is already severe, dielectric loss within antenna materials must remain minimal. Low-loss substrates such as RO3010, RT/duroid 5880, and alumina help preserve radiation efficiency and limit thermal dissipation, whereas higher-loss polymers must be used sparingly or restricted to thin encapsulation layers. These considerations tightly couple electromagnetic design to material choice; bandwidth, efficiency, SAR compliance, and long-term stability cannot be treated independently. The frequency-dependent loss tangent also influences the effective quality factor, linking substrate selection to bandwidth behavior in wideband and multiresonant implant designs under dispersive tissue loading. In summary, electromagnetic design for implantable antennas is inseparable from materials engineering since substrate permittivity, encapsulation properties, loss tangent, and interface quality jointly determine how energy is stored, radiated, and absorbed in vivo.

CORE SUBSTRATE MATERIALS IN IMPLANTABLE ANTENNAS

Core substrates govern electromagnetic confinement, radiation efficiency, and mechanical integration of implantable antennas. High-permittivity PTFE–ceramic laminates are widely used for electrically small MICS/ISM implants because they combine high dielectric constant, moderate loss, manufacturability, and compatibility with thin multilayer stacks. Their relatively high permittivity ($\varepsilon_r \approx 10$) enables significant miniaturization of patches and loops while maintaining acceptable radiation efficiency within lossy tissue environments [22], [24], [36], [37], [38], [43], [48], [51]. Since the guided wavelength scales approximately as $\lambda_g \approx \lambda_0/\sqrt{\varepsilon_{\text{eff}}}$, RO3010 and RO6010 reduce the guided wavelength by nearly a factor of 2–3 compared with FR4 ($\varepsilon_r \approx 4.4$), thereby supporting subcentimeter antennas at 0.915 and 2.45 GHz [20], [22], [24], [36], [38]. Recent compact and high-data-rate implantable antenna designs, including

TABLE 2. MICS AND MEDRADIO FREQUENCY ALLOCATIONS [13], [14].

Band	Range (MHz)	Representative Implantable Applications
MICS	402–405	Low-power implant telemetry for pacemakers, ICDs, neurostimulators, and pressure sensors
MedRadio (core)	401–406	Telemetry and closed-loop control in implants; neural stimulation and monitoring links
MedRadio (extended)	413–419, 426–432, 438–444, 451–457	Implant-to-wearable relays, redundant telemetry, and distributed body-area networks

TABLE 3. DIELECTRIC PROPERTIES OF HUMAN TISSUES AT IMD BANDS (37° C) [15].

	MICS (402 MHz)			ISM (2.45 GHz)		
Tissue	ε_r	σ (S/m)	tanδ	ε_r	σ (S/m)	tanδ
Skin (wet)	46.7	0.69	0.661	38.1	1.441	0.278
Muscle	57.1	0.8	0.626	52.8	1.705	0.237
Fat	5.6	0.04	0.319	5.29	0.102	0.142
Cortical bone	12.5	0.08	0.286	11.4	0.394	0.254
Brain (gray)	55.5	0.5	0.403	48.9	1.07	0.161
Brain (white)	37	0.29	0.35	37	0.9	0.178
Blood	61	1.1	0.806	58.2	2.15	0.271
Bone marrow	12	0.06	0.224	11	0.25	0.167
Vitreous humor	74.2	1.83	1.103	65	2.1	0.237
Lung (inflated)	24	0.25	0.466	22	0.4	0.133

Note: Values from the Gabriel tissue database [15]. Loss tangent computed as $\tan\delta = \sigma/(2\pi f \varepsilon_0 \varepsilon_r)$ [16], [17].

multiple-input, multiple-output (MIMO), dual-band wireless power transfer (WPT), and in-band full-duplex implementations, continue to rely on such high-ε_r material platforms for miniaturization and stable in-body performance [52], [53], [54], [55].

However, high-ε_r loading also introduces surface-wave and link-budget penalties since classical microstrip theory shows that surface-wave excitation increases with substrate permittivity and thickness and acts as a nonradiating loss mechanism that degrades radiation efficiency, polarization performance, and realized gain in lossy tissue environments [20]. Thus, although RO3010/RO6010-class laminates support miniaturization, they also strengthen lateral bound fields compared with low-ε_r substrates such as RT/duroid 5880. Ultrathin (≈ 0.127 mm) high-ε_r layers partly reduce this penalty, explaining their use in compact MIMO capsule systems [53]. In lossy tissue, surface-bound energy is further dissipated through conduction and dielectric loss rather than useful far-field radiation [2], [3], [30], [39]. This mechanism is also visible in implantable reports where surface or impedance-engineered modes are deliberately controlled rather than ignored; the reactive impedance surface (RIS)-loaded dual-band implant in [43] uses surface-wave generation to obtain circular polarization (CP) operation and subsequently evaluates link margin, while quality-factor-based patch analysis shows that high-loss tissue turns the implanted microstrip patch antenna into a very low-Q_T lossy resonator [39]. In practical designs, this penalty appears as depressed realized gain and reduced link margin; for example, MTM-assisted gain recovery of about 3 dB was reported after a low-gain flexible implant response [35], and dual-band scalp implants at 915/2,450 MHz reported peak gains of −28.5/−22.8 dBi with link-budget evaluation [38].

At the system level, this penalty enters directly through the realized-gain term in the Friis-based implant link budget [21], where every 10 dB of reduction in radiation efficiency or realized gain translates into roughly 10 dB of additional loss in available link margin. Reported compact implants confirm this scale; an ultra-thin RO3010 four-port MIMO capsule antenna has a measured peak gain of about −21.2 dBi [53]; a miniaturized RO3010 dual-band implant reports gains of about −21.8 and −19.2 dBi at 915 MHz and 2.4 GHz, respectively [54]; and a compact cardiac implant reports radiation efficiency near 0.1% with peak gain around −24.9 dBi [61]. Therefore, high-ε_r laminates are useful for miniaturization, but their surface-wave and tissue-absorption penalties must be mitigated through substrate thinning, low-loss laminates, full-ground-plane control, metasurface/RIS loading, or multilayer impedance engineering [43], [57], [58].

The same near-field confinement has direct safety implications because, for a fixed antenna–tissue configuration, SAR increases with local electric-field intensity and tissue conductivity and scales approximately linearly with input power. Therefore, allowable input power is commonly estimated by scaling the reported normalized SAR to the IEEE/ICNIRP exposure limits [18], [19]. Reported high-ε_r implant examples show that SAR-constrained allowable power is often limited to only a few milliwatts in compact high-permittivity implants across both sub-GHz and 2.45 GHz operation. At 915 MHz, a wideband CP implant reported a maximum SAR of 778 Wkg^{-1} for 1 W input, limiting allowable power to about 2.05 mW [41]. At 2.45 GHz, compact high-ε_r implants report normalized 1-g SAR values of 697.5–790.7 Wkg^{-1} and allowable input powers of only about 1.86–2.3 mW, depending on the tissue model and packaging [68], [79]. Similarly, a dual-band implant reported 1-g/10-g SAR values of 473/49.3 Wkg^{-1} at 2.4 GHz, corresponding to allowable powers of 3.38/40.56 mW [78]. For multiport or WPT-oriented implants, SAR remains equally design-limiting; a cubic MIMO implant reported four-port 1-g average SAR values above 1,100 Wkg^{-1} at 2.45 GHz for 1 W excitation [58], while a dual-band WPT rectenna demonstrated SAR-compliant operation with peak SAR values of 1.22 and 0.90 Wkg^{-1} at 915 MHz and 2.45 GHz, respectively [62]. Thus, high-ε_r and ceramic-loaded stacks should be evaluated through normalized SAR, allowable input power, radiation efficiency, and link margin rather than compactness or impedance matching alone.

To mitigate these penalties, reported designs use ultra-thin high-ε_r laminates, low-loss PTFE substrates such as RT/duroid 5880, full-ground or ground-radiating layouts, and resonator-based or volumetric structures such as DRAs and cubic MTM/MIMO systems [58], [59], [62], [63], [75]. In these hybrid stacks,

TABLE 4. SAR LIMITS FOR HUMAN EXPOSURE [18], [19]

Standard	Mass	Quantity	Limit
IEEE C95.1			
Head/torso (1999)	1 g	SAR	1.6 W/kg
Limbs (1999)	1 g	SAR	4 W/kg
Head/torso (2005/2019)	10 g	SAR	2 W/kg
Limbs (2005/2019)	10 g	SAR	4 W/kg
Whole body	—	SAR	0.08 W/kg
Far-field (≥6 GHz)	Area	Absorbed Power density	10 W/m^2
ICNIRP 2020			
Head/torso	10 g	SAR	2 W/kg
Limbs	10 g	SAR	4 W/kg
Whole body	—	SAR	0.08 W/kg
Far-field (≥6 GHz)	4 cm^2	Absorbed Power density	10 W/m^2

the low-loss or volumetric region reduces dissipative loading, while the high-ε_r region provides miniaturization and modal control.

An increasingly prominent trend is the transition from rigid laminates to flexible and conformal substrates. Soft polymers such as PDMS and silicone ($\varepsilon_r \approx 2.5-3.0$) enable organ-wrapping, capsule, and injectable geometries [31], [32], [33]. Their low permittivity requires miniaturization through meandering, capacitive tuning, or high-ε_r loading. Thin-film polyimide and polyether ether ketone (PEEK) substrates (50–100 μm) support compact loop, MIMO, and injectable systems with stable electrical and mechanical behavior [29], [40], [65], [66], [76], [80]. High-resistivity silicon (HRS) offers extreme size reduction at 915 MHz due to its high permittivity ($\varepsilon_r \approx 11.9$), but strong dielectric and surface-wave losses can reduce radiation efficiency below 0.1% in deep tissue [47]. Meanwhile, 3D-printed biocompatible MED610 ($\varepsilon_r \approx 2.8$, $\tan\delta \approx 0.0035$) enables volumetric CP geometries, including hemispherical radiators for deeply embedded implants [80]. Table 5 summarizes this tradespace; high-ε_r PTFE laminates dominate compact MICS/ISM designs [22], [23], [24], [28], [36], [37], [38], [39], [41], [43], [44], [45], [46], [48], [51], [53], [54], [55], [57], [61], [62], [66], [72], [74], [77], [79], flexible polymers enable conformal and injectable systems [31], [32], [40], [42], [59], [65], and semiconductor or 3D-printed substrates support specialized compact or volumetric implementations [47], [80].

MTM-ENHANCED SUBSTRATES

MTM-inspired substrates have gradually become practical tools for pushing past the usual tradeoffs among size, bandwidth, and efficiency in implantable antennas. When a thin magneto–dielectric layer is introduced, even one only a few micrometers thick, the effective permeability rises above unity, and the antenna can collapse in electrical size without forcing the electric field to crowd tightly into lossy tissue. A representative example appears in [23], where a roughly 5-μm Ni–Co ferrite coating was sputtered onto a RO3010 laminate ($\varepsilon_r \approx 10.2$). Despite its minimal thickness, the film shifted the resonant behavior enough to yield a noticeably smaller 2.45-GHz radiator while keeping the total stack height near 1.3 mm. What this approach achieves, in practical terms, is a redistribution of stored energy; more of it is held magnetically, and less relies on the strongly capacitive fields that typically elevate loss and SAR in biological tissue. As a result, magneto–dielectric loading can relax the pressure to use extremely high-ε_r substrates and opens an additional path toward compact but still efficient implanted radiators.

Several designs introduce periodic resonant elements—including complementary split-ring resonators (CSRRs), RISs, and electrically small volumetric resonators to tailor the effective impedance and dispersion within the tissue environment. RISs employ engineered inductive–capacitive grids to tune the surface impedance seen by the antenna, often improving matching or enabling multiband operation without altering the core geometry. A metamaterial-inspired slot-loaded configuration reported in [33] achieves a broad 1.3–3.5–GHz impedance bandwidth centered around 2.45 GHz on a silicone substrate, while [35] employs a patterned Kapton-based superstrate over a high-ε_r RO6010 patch to recover gain and axial-ratio bandwidth otherwise degraded under tissue loading.

RIS-based electromagnetic tuning has been directly demonstrated for compact implantable antennas. In [43], a RO3010-based RIS layer is integrated beneath a meandered loop, producing dual-band circular polarization at 920 MHz and 2.45 GHz within a $10 \times 10-\text{mm}^2$ footprint and maintaining robust performance under bending. Volumetric metamaterial loading is also reported for cubic resonators, where zirconia-loaded RT5880 blocks support circular polarization, enhanced isolation, and stable multiband MIMO behavior [52], [58], [63]. It is noted that such high-permittivity and metamaterial loading typically increases the effective quality factor, resulting in reduced fractional bandwidth and highlighting the tradeoff

TABLE 5. CORE SUBSTRATE CATEGORIES IN IMPLANTABLE ANTENNAS.

Category	Examples	EM/Mechanical Role
High-ε_r laminates	RO3010, RO3210, RO6010, RT6010LM, TMM13i	Rigid substrates for strong miniaturization and stable MICS/ISM operation
Low-ε_r PTFE	RT5880, ULTRALAM 3850HT, RO3003	Low-loss high-efficiency platforms for wideband and conformal designs
FR4 + DRA loading	FR4 + dielectric resonators	Low-cost support; DRA enables miniaturization and gain enhancement
Flexible elastomers	PDMS, silicone, HAp/PDMS	Soft and conformal substrates for organ-wrapping and flexible implants
Thin polymer films	Polyimide, Kapton, PI/PEEK	Ultra-thin flexible cores for loops, CPW-fed and injectable antennas
Biocompatible polymers	MED610	Rigid shells for capsules and 3D geometries with good in vivo stability
Semiconductor/ceramic	HRS Si, alumina	Extreme miniaturization; higher loss reduces efficiency

between miniaturization and achievable data-rate performance. Metasurfaces have also been investigated as add-on layers to manipulate radiation patterns, link margin, and local SAR distribution. A compact 2.45–GHz circularly polarized antenna in [72] employs a RO6010 substrate patterned with subwavelength slots to achieve a footprint below $0.05\lambda_0^3$ while maintaining adequate bandwidth. In [76], metasurfaces are identified as a prospective pathway for enhancing tissue-independent MIMO performance, beam-shaping, and energy-harvesting integration in injectable antennas.

Overall, MTM-enhanced substrates remain less common than purely dielectric laminates, but they enable extreme miniaturization, circular polarization, and improved inter-port isolation. Table 6 summarizes these strategies, from magneto–dielectric films [23] and slot-loaded/CSRR substrates [33], [35], [42] to RIS and epsilon-near-very-large (EVL)/MTM structures [43], [58], [63], with recent metasurface designs extending miniaturization and pattern control [72], [76].

ENCAPSULATION, COATINGS, AND BIOCOMPATIBILITY LAYERS

Encapsulation materials form the first physical and electromagnetic interface between an implantable antenna and the surrounding biological tissue. Beyond protecting conductors and substrates from ionic fluids and corrosion, encapsulation layers strongly influence impedance stability, near-field distribution, and SAR. As summarized in Table 7, most implantable antenna designs rely on three encapsulation strategies: bioceramic coatings, polymeric shells, and hybrid multilayer stacks. Each category represents a different balance between electromagnetic stability, mechanical robustness, and long-term biocompatibility, and the choice is often dictated by implantation depth, expected lifetime, and mechanical constraints.

Bioceramic encapsulants—most commonly alumina ($\varepsilon_r \approx 9.2$–$9.8$) and zirconia ($\varepsilon_r \approx 27$)—are widely used in long-term and deep implants because of their chemical inertness, mechanical hardness, and stable dielectric response. Thin alumina layers are frequently introduced as buffers between high-ε_r PTFE–ceramic substrates and surrounding tissue, helping to stabilize resonance and preserve circular polarization across MICS and ISM bands [22], [38], [48]. However, bioceramics are not electromagnetically neutral; their relatively high permittivity adds dielectric loading, and small variations in coating thickness can shift resonance or narrow bandwidth, particularly in ultra-compact CP antennas. For this reason, bioceramic

TABLE 6. MTM-ENHANCED SUBSTRATE CATEGORIES IN IMPLANTABLE ANTENNAS.

Category	Implementation	EM role
Magneto–dielectric films	Ni–Co ferrite (~5 μm) on RO3010	Increases μ_r and reduces resonant size with limited ε_r increase [23]
Slot/CSRR MTM substrates	Periodic slots, CSRRs in silicone or polyimide	Controls dispersion; enables wide bandwidth and stable patterns under tissue loading [33], [35], [42]
RIS loading	RO3010 RIS grids with meandered loops	LC surface tuning for dual-band CP (0.92/2.45 GHz) in compact layouts [43]
Volumetric MTM/EVL	Zirconia-loaded RT5880 cubes, 3D resonators	EVL behavior; improves CP stability, isolation, and multiband MIMO [58], [63]
Metasurface miniaturization	RO6010 with periodic subwavelength slots	Extreme miniaturization ($<0.05\lambda_0^3$) with maintained CP bandwidth [72]
Tunable MTM platforms	Polyimide-based flexible MIMO arrays	Supports reconfigurability, beam shaping, and energy-harvesting integration [51], [76]

TABLE 7. ENCAPSULATION AND COATING CATEGORIES IN IMPLANTABLE ANTENNAS.

Category	Materials (ε_r)	Thickness	EM/functional role
Bioceramic coatings	Alumina (9.4–9.8), zirconia (27)	0.02–0.5 mm	Hermetic sealing, long-term stability, CP preservation; reduces detuning in tissue
Elastomeric encapsulants	PDMS (2.7–3), Silastic (3.3)	0.2–2 mm	Flexible coatings; smooth field distribution and reduced SAR
Rigid polymer shells	PEEK (3.2), MED610 (2.8)	0.05–0.15 mm	Robust housings for capsules and 3D structures with minimal detuning
Hybrid multilayer coatings	High-ε_r core + PI/PDMS/ gypsum/ acrylic/graphene	Structure-dependent	Combined tuning of IBW, ARBW, and SAR; acts as buffer, lens, or biointerface

encapsulation must be co-designed as part of the radiating structure rather than treated as passive packaging.

Polymeric encapsulants provide a complementary approach. Materials such as PDMS and medical-grade silicone ($\varepsilon_r \approx 2.7–3.0$) combine low permittivity with very low Young's modulus, making them well suited for soft-tissue interfaces and conformal or injectable geometries [31], [57], [67], [71]. These elastomers smooth dielectric transitions at the tissue boundary, redistribute near fields, and often reduce peak SAR while maintaining stable matching in heterogeneous tissue environments. In contrast, rigid polymer shells such as PEEK and additively manufactured MED610 offer mechanically robust housings for capsule endoscopes and hemispherical radiators [40], [47], [80]. Their moderate permittivity introduces less detuning than bioceramics for comparable thickness, simplifying matching in ISM-band systems.

An increasing number of designs adopt hybrid multilayer encapsulation strategies, in which a thin high-ε_r core (e.g., RO6010 or a ceramic dielectric resonator) is combined with an outer polymeric or acrylic layer to jointly control bandwidth, SAR, and mechanical reliability [36], [39]. In several cases, the encapsulation itself contributes directly to the electromagnetic function: alumina superstrates acting as dielectric lenses to recover realized gain [56], monolithic polymer platforms integrating both radiator and package [76], or bioactive coatings such as gypsum ($CaSO_4\ 2H_2O$) providing a bone-compatible dielectric interface for antennas mounted on metallic hip implants [82]. The trends highlighted in Table 7 underscore a central conclusion; encapsulation materials are not merely protective layers but electromagnetically active elements that must be optimized alongside the substrate and radiator. Designs that explicitly co-optimize encapsulation thickness, permittivity, loss tangent, and mechanical compliance consistently demonstrate improved robustness to anatomical variation, implantation depth, and long-term in vivo operation, although thicker coatings, while improving isolation, can also detune resonance and reduce bandwidth if not co-designed. Complementary surface-engineering studies on titanium-based implants further show that controlled formation of nanostructured TiO_2 layers can enhance corrosion resistance and biological response without degrading electromagnetic stability [83], [84]. Such surface treatments are increasingly relevant for implantable antenna ground planes and housings, where electrochemical reliability and biocompatibility are as important as radiation performance. In summary, effective encapsulation design is inseparable from electromagnetic design in implantable antennas. Treating encapsulation as an integral and material-driven component— rather than as an afterthought—remains essential for achieving safe, stable, and clinically viable implantable wireless systems.

CONDUCTIVE AND GROUND MATERIALS

Conductive traces and ground planes play a dual role in implantable antennas; they define current distribution and radiation efficiency while also acting as long-term electrochemical interfaces with biological tissue. Therefore, beyond bulk conductivity, chemical inertness, corrosion resistance, adhesion to dielectrics, and galvanic compatibility with surrounding materials determine both electromagnetic stability and clinical safety. Table 8 summarizes the principal conductive and ground material categories used in implantable antennas.

Conventional high-conductivity metals, mainly copper and gold, remain the most widely used metallization options. Copper is prevalent in research prototypes because of its high conductivity and compatibility with PTFE–ceramic laminates, but it is not intrinsically biocompatible and oxidizes in physiological environments. Therefore, copper traces must be fully encapsulated using Parylene C, PDMS, epoxy, or multilayer polymer barriers to prevent ion release and corrosion. Gold, by contrast, offers excellent chemical inertness and long-term electrochemical stability, making it more suitable for chronic implants despite its slightly lower conductivity. Platinum–iridium and titanium nitride appear in applications where radiating elements are integrated with electrodes, trading conductivity for stronger adhesion and long-term biocompatibility [33].

Bio-metallic ground planes, particularly titanium-based alloys, form a distinct and increasingly important category. Ti–6Al–4V and related alloys are widely used as implant housings and structural grounds because they combine biocompatibility, mechanical strength, and corrosion resistance [89]. Although their electrical conductivity is much lower than that of copper or gold, titanium grounds can function

TABLE 8. CONDUCTIVE AND GROUND MATERIAL CATEGORIES IN IMPLANTABLE ANTENNAS.

Category	Implementation	Functional role
High-conductivity metals	Cu, Au on PTFE/ceramic	Cu for prototyping (encapsulation required); Au for stable long-term conduction; used in CP patches and loops
Bio-metallic grounds	Ti–6Al–4V	Biocompatible structural ground; PDMS/HAp coatings stabilize current paths and reduce ion migration
Flexible/composite conductors	Au nanolayers, Ag–PDMS, graphene films	Flexible, stretchable conductors; require encapsulation; enable conformal and multifunctional implants
3D metallization	Metal plating on RT5880 cubes, MED610 shells	Volumetric grounds for EVL/MTM and CP antennas; improve isolation, pattern control, and multiband operation

effectively when combined with dielectric buffer layers such as PDMS or hydroxyapatite. These buffers moderate the metal–tissue interface, stabilize current paths, reduce mutual coupling, and support predictable back-radiation [31], [32], [82]. Surface-engineered titanium, especially anodized or nanostructured TiO_2, further improves electrochemical stability and biological response, making titanium-based structures attractive for load-bearing implants that also act as RF grounds [83], [84], [86]. In contrast, stainless steel alloys such as 316L are less attractive for RF grounding because of higher magnetic loss and corrosion susceptibility unless fully sealed.

Emerging composite and flexible conductors address the mechanical demands of conformal and injectable implants. Silver–PDMS composites, ultra-thin gold films, graphene sheets, and carbon nanotube networks can provide low sheet resistance while tolerating bending, twisting, and repeated mechanical cycling. These materials enable antenna architectures that are difficult to realize with rigid metal foils, including intraoral sensors, soft implants, and stretchable platforms. Their use, however, requires careful encapsulation to prevent ion migration and cytotoxicity, and long-term fatigue data remain limited. Recent graphene-based implantable antenna immunosensors also highlight the potential of multifunctional conductive layers that combine RF performance with biochemical sensitivity [81]. At 2.45 GHz, the limited skin depth of silver–PDMS composites increases effective ohmic dissipation relative to bulk metals, while repeated strain can gradually degrade the electrical performance of both silver–PDMS composites and ultra-thin gold layers, affecting radiation efficiency, link budget, and long-term implant reliability.

Across all conductor categories, electrical performance is inseparable from chemical stability. Corrosion, delamination, and galvanic reactions alter surface impedance, detune resonance, and may increase SAR by concentrating current at material interfaces. Therefore, multilayer protection schemes using metallic traces, adhesion promoters, and polymer or ceramic diffusion barriers are essential for long-term operation [2], [3], [4]. Overall, conductor selection is shifting from conductivity alone toward chemically stable and mechanically compliant systems; copper remains useful for prototyping, gold and PtIr support chronic implantation, titanium alloys provide robust biocompatible grounds, and composite conductors enable flexible or injectable antenna architectures.

CHALLENGES AND FUTURE RESEARCH DIRECTIONS

As summarized in Table 9, recent progress in implantable antenna technology is increasingly driven by material co-design rather than geometry alone. Substrate permittivity, conductor choice, and encapsulation stacks now jointly determine achievable miniaturization, radiation efficiency, SAR compliance, and long-term reliability. Despite these advances, several material-driven challenges continue to limit the translation of laboratory prototypes into clinically robust implant platforms. A primary challenge remains the tradeoff between electrical miniaturization, efficiency, and SAR. High-ε_r PTFE–ceramic laminates and semiconductor dielectrics enable aggressive size reduction but concentrate near fields in lossy tissue, often reducing realized gain and tightening

TABLE 9. PRESENT AND EMERGING MATERIALS FOR IMPLANTABLE ANTENNAS.

Material/Family	ε_r	tanδ	Flexibility	Biocomp.	Role
High-ε_r PTFE laminates (RO3010/3210/6010)	~10	~0.002–0.003	Rigid	Encap.	Miniaturized MICS/ISM substrates
RO3003	~3	~0.001	Rigid	Encap.	Low-loss moderate-ε_r core
RT5880	~2.2	$< 10^{-3}$	Rigid	Encap.	Ultra-low-loss, high-efficiency designs
LCP (ULTRALAM)	~3.1	~0.002	Flex.	Good	Conformal multilayer implants
Polyimide	3–3.5	0.005–0.01	Flex.	Coated	Ultra-thin flexible/injectable systems
PDMS/silicone/MED610	2.7–3	~0.01	Very flex.	Excellent	Encapsulation, SAR buffering, comfort
Alumina/zirconia/ATZ/HAp	9–25	< 0.002	Rigid	Excellent	Hermetic housings, DRAs, bone implants
LTCC ceramics	5–70	$< 5 \times 10^{-3}$	Rigid	Coated	3D multilayer/mmWave DRAs
Gypsum ($CaSO_4$)	~2.7	Low	Rigid	Good	Bone-compatible dielectric layer
Perovskite ceramics	20–100+	$\lesssim 10^{-3}$	Rigid	Under study	High-Q compact DRA cores
TiO_2 (rutile)	80–100	$< 10^{-3}$	Rigid	Excellent	mmWave DRA cores and coatings
Ceramic–polymer composites	5–20	0.005–0.02	Flex.	Varies	Gradient-index/SAR control
Graphene hybrids	~3.3	–	Flex.	Promising	Flexible biointerfaces, sensing
Biodegradable polymers	2.5–4	0.01–0.03	Var.	Biores.	Transient diagnostic implants

Biocomp.: biocompatibility; Encap.: encapsulation required; Flex.: flexible; Var.: variable; Biores.: bioresolution (or biodegradable/bioresorbable).

SAR margins [22], [36], [47], [72], [73]. As reflected in Table 9, magneto–dielectric and metamaterial-inspired substrates partially mitigate this tradeoff by redistributing stored energy or tailoring surface impedance [23], [33], [43], [58], [63]. However, many current implementations remain rigid, narrowband, or difficult to integrate with soft encapsulation. Progress toward clinically viable systems will require low-loss, bio-inert, and mechanically compliant magnetic or metamaterial composites that can be laminated or coprinted with flexible substrates while maintaining stable ε_r, μ_r, and low dielectric loss.

Robustness to anatomical variability is a second, closely related limitation. Implantable antennas operate in tissue environments whose dielectric properties vary with anatomy, patient physiology, healing processes, and implant migration. Changes in fat–muscle composition or encapsulation thickness can detune impedance and degrade link margin. Current mitigation strategies—dielectric buffering, RIS layers, reconfigurable grounds, and multiband or MIMO geometries—improve tolerance to tissue variation but remain optimized for limited phantom models [43], [66], [76]. Emerging workflows based on fast surrogate modeling, multiobjective optimization, and closed-loop calibration using backscattered or physiological feedback offer promising routes toward designs inherently robust to anatomical uncertainty.

Long-term biostability and lifetime reliability represent a third critical bottleneck. While Table 9 highlights a practical palette of materials for chronic implants (alumina, zirconia, PEEK, PDMS, medical-grade silicones, and stable metallizations), systematic data on hydrolysis, moisture ingress, microcracking, and interfacial delamination over multiyear lifetimes remain scarce. These degradation mechanisms often couple with corrosion of thin metal traces and galvanic interactions between dissimilar materials, gradually altering surface impedance and resonance. Broader biomedical materials research points to underexplored opportunities for antenna stacks, including bio-inert polymers (ultra-high-molecular-weight polyethylene, polyethylene terephthalate, and advanced fluoropolymers) [90], [93], [96], [98], bioactive ceramics and glasses [HAp, Ca–P systems, zirconia, alumina–zirconia toughened composite (ATZ)] [87], [97], [94], and advanced surface coatings such as TiN, diamond-like carbon, and hydrogels, and antimicrobial layers [92]. In parallel, next-generation titanium alloys and nanostructured TiO_2 layers offer attractive solutions for implant housings and RF grounds requiring combined mechanical integrity, corrosion resistance, and electrochemical stability [83], [84], [85], [88], [89].

Finally, materials enabling higher-frequency and multifunctional implants are becoming increasingly important. Operation in the 24-GHz ISM band and beyond enables sub-mm apertures and large bandwidths but suffers from increased tissue attenuation, favoring shallow ocular, dental, or dermal implants. In this regime, low-loss material platforms from microwave and millimeter-wave (mmWave) engineering dominate the design space. As indicated in Table 9, LTCC substrates and engineered perovskite ceramics provide high-Q dielectric building blocks for compact DRAs [16], [91]. Rutile-phase

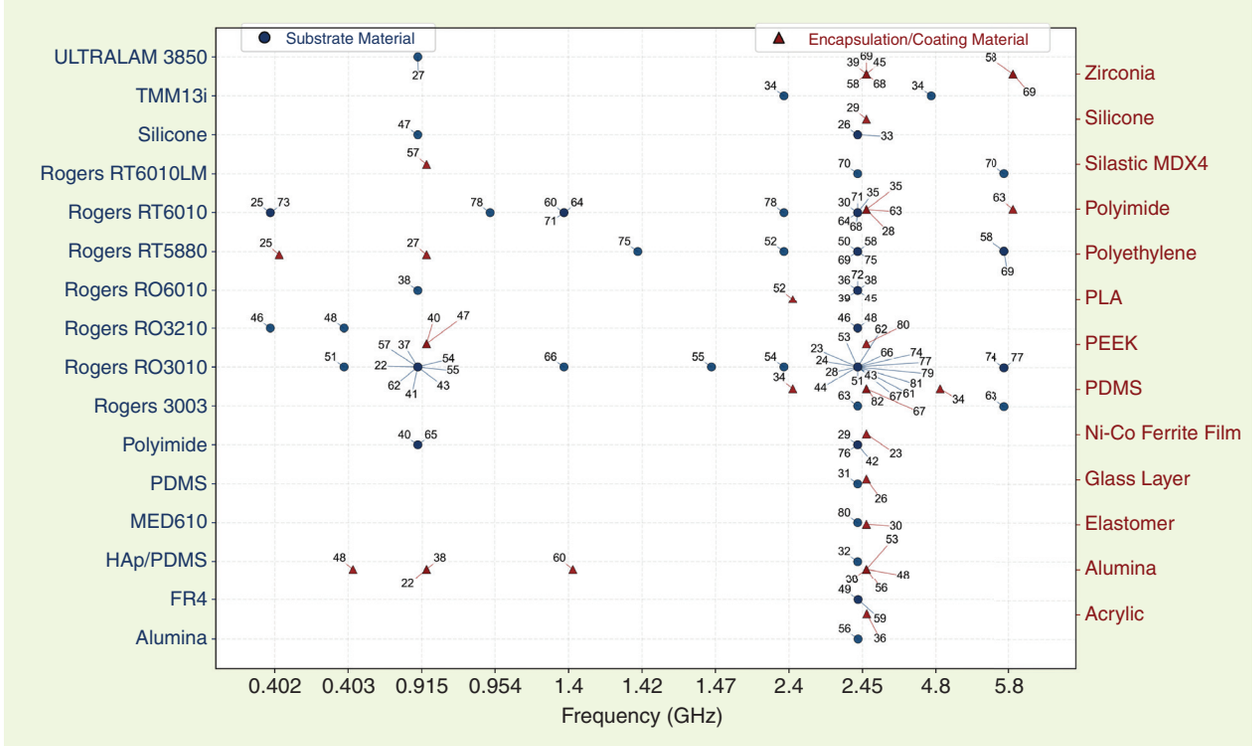


FIGURE 3. Material-frequency scatter map of the surveyed implantable antenna studies (2015–2025) (labels indicate reference numbers).

TiO_2 is particularly promising, combining very high permittivity, extremely low dielectric loss, and established biocompatibility, allowing it to function both as a resonant core and as a stable bioceramic surface layer [83], [84], [97]. These emerging materials significantly expand the design space for mmWave implantable antennas, where conductor loss and RF heating dominate performance limits. Figure 3 provides a material-frequency view of the reviewed implantable antenna literature and highlights a clear evolution from high-ε_r ceramic/PTFE laminates for miniaturization toward flexible polymers, hybrid composites, and biocompatible coatings for conformal integration, improved biostability, and multifunctional higher-frequency operation. Overall, these challenges show that implantable antennas should be treated as material-engineered subsystems rather than standalone radiators. Future platforms will rely on hybrid stacks combining high-ε_r cores for miniaturization, low-ε_r buffers for SAR control, bioceramic or engineered coatings for long-term stability, and magnetic or metasurface elements for bandwidth and polarization control. Thus, electromagnetic behavior is governed as much by the engineered material stack as by metallic geometry. Tables 5–9 further show a transition from high-permittivity ceramic substrates at sub-GHz bands toward flexible polymers and hybrid materials at higher frequencies, reflecting evolving priorities in miniaturization, bandwidth, and biocompatibility.

CONCLUSION

This review highlights that material selection is central to the miniaturization, efficiency, biostability, and clinical viability of implantable antennas. High-ε_r PTFE–ceramic laminates enable size reduction, but their surface-wave confinement, realized-gain penalty, and SAR-limited input power must be jointly evaluated with the link budget. Low-loss substrates such as RO3003 and RT/duroid 5880 improve radiation efficiency, flexible polymers (polyimide, LCP, and PDMS) enable conformal integration, and bioceramics (alumina and zirconia) provide durable encapsulation. Emerging platforms, including rutile TiO_2, perovskite microwave ceramics, LTCC glass–ceramics, ceramic–polymer composites, and biodegradable polymers, broaden the design space toward higher frequencies and improved bio-integration, while DRAs offer lower conductor loss and reduced RF heating. Nevertheless, most clinical implants still rely on MedRadio/MICS and inductive telemetry because of robust tissue penetration and low power demand. Bridging laboratory advances to clinical adoption will require low-loss, bio-stable, and hybrid multimaterial architectures that jointly optimize electromagnetic performance and patient safety.

ACKNOWLEDGMENT

This study (under CanDia CUP E13C24002390006) was supported by the European Union – NextGenerationEU, under the Italian National Recovery and Resilience Plan (NRRP), Mission 4 Component 2 Investment 1.2, funding scheme "Young Researchers" (D.D. 201 del 3.7.2024). Ladislau Matekovits is the corresponding author.

AUTHOR INFORMATION

Sumer Singh Singhwal (sumer.singhwal@polito.it) is with the Department of Electronics and Telecommunications, Politecnico di Torino, 10129 Turin, Italy. The author's research interests include implantable antennas, dielectric resonator antennas, bioelectromagnetics, and wireless health-care systems. The author is a Horizon Europe Seal of Excellence recipient. The author is a Senior Member of IEEE.

Ladislau Matekovits (ladislau.matekovits@polito.it) is with the Department of Electronics and Telecommunications, Politecnico di Torino, 10129 Turin, Italy, Istituto di Elettronica e di Ingegneria dell'Informazione e delle Telecomunicazioni, National Research Council of Italy, 10129 Turin, Italy, and Department of Measurements and Optical Electronics, University Politehnica Timisoara, 300006 Timisoara, Romania. The author is an associate professor and former Marie Curie Fellow. The author's research interests include computational electromagnetics, metamaterials, implantable antennas, and reconfigurable antenna systems. The author is a Senior Member of IEEE.

Ildiko Peter (ildiko.peter@umfst.ro) is a full professor with the Department of Industrial Engineering and Management, Faculty of Engineering and Information Technology, George Emil Palade University of Medicine, Pharmacy, Science, and Technology of Târgu Mureş, 540139 Târgu Mureş, Romania. The author's research interests include biomaterials, materials engineering, and advanced materials for health-care applications.

REFERENCES

[1] "Implantable medical devices market (2025 Edition), market research report." Accessed: Nov. 14, 2025. [Online]. Available: https://www.thebusinessresearchcompany.com/report/implantable-medical-devices-market

[2] A. Kiourti and K. S. Nikita, "A review of implantable patch antennas for biomedical telemetry: Challenges and solutions [Wireless Corner]," *IEEE Antennas Propag. Mag.*, vol. 54, no. 3, pp. 210–228, Jun. 2012, doi: 10.1109/MAP.2012.6293992.

[3] A. Kiourti and K. S. Nikita, "Implantable antennas: A tutorial on design, fabrication, and In Vitro/In Vivo testing," *IEEE Microw. Mag.*, vol. 15, no. 4, pp. 77–91, Jun. 2014, doi: 10.1109/MMM.2014.2308765.

[4] A. Kiourti and K. S. Nikita, "A review of in-body biotelemetry devices: Implantables, ingestibles, and injectables," *IEEE Trans. Biomed. Eng.*, vol. 64, no. 7, pp. 1422–1430, Jul. 2017, doi: 10.1109/TBME.2017.2668612.

[5] M. M. Soliman et al., "Review on medical implantable antenna technology and imminent research challenges," *Sensors*, vol. 21, no. 9, 2021, Art. no. 3163, doi: 10.3390/s21093163.

[6] A. Kiourti et al., "Next-generation healthcare: Enabling technologies for emerging bioelectromagnetics applications," *IEEE Open J. Antennas Propag.*, vol. 3, pp. 363–390, 2022, doi: 10.1109/OJAP.2022.3162110.

[7] M. R. K. M. Samy and A. Gudipalli, "A review on miniature bio-implant antenna performance enhancement and impact analysis on body fluids in medical application," *Meas.: Sensors*, vol. 28, 2023, Art. no. 100849.

[8] A. Mohan and N. Kumar, "Implantable antennas for biomedical applications: A systematic review," *Biomed. Eng. Online*, vol. 23, no. 1, 2024, Art. no. 87, doi: 10.1186/s12938-024-01277-1.

[9] M. Benaissa, A. Chaabane, H. Attia, and I. Al-Naib, "Innovations and challenges in RF antenna technologies for implantable medical devices communication," *IEEE J. Microwaves*, vol. 5, no. 3, pp. 526–542, May 2025, doi: 10.1109/JMW.2025.3555480.

[10] M. Jasim, A. J. A. Al-Gburi, M. Hanif, Z. A. Dayo, M. M. Ismail, and Z. Zakaria, "An extensive review on implantable antennas for biomedical applications: Health considerations, geometries, fabrication techniques, and challenges," *Alexandria Eng. J.*, vol. 112, pp. 110–139, Jan. 2025, doi: 10.1016/j.aej.2024.10.105.

[11] U.S. Federal Communications Commission, "Operating frequencies for Industrial, Scientific, and Medical (ISM) equipment," *Code of Federal Regulations, Title 47, Chapter I, Subchapter A, Part 18, Subpart C, §18.301*, Washington, DC, USA: National Archives and Records Administration,

Oct. 2025. Accessed: Jan. 14, 2026. [Online]. Available: https://www.ecfr.gov/current/title-47/chapter-I/subchapter-A/part-18/subpart-C/section-18.301
[12] H. Mazar (Madjar), "International, regional and national regulation of SRDs," in *Proc. ITU Workshop on Short Range Devices (SRDs) and Ultra Wide Band (UWB)*, International Telecommunication Union, Geneva, Switzerland, Jun. 2014. Accessed: Jan. 14, 2026. [Online]. Available: https://www.itu.int/en/ITU-R/study-groups/workshops/RWP1B-SRD-UWB-14/Presentations/International%2C%20regional%20and%20national%20regulation%20of%20SRDs.pdf
[13] Federal Communications Commission, "Medical Device Radio communications Service (MedRadio)," 47 C.F.R. Part 95 Subpart E, Wireless Telecommunications Bureau, Washington, DC, USA. Accessed: Jan. 14, 2026. [Online]. Available: https://www.fcc.gov/medical-device-radio-communications-service-medradio
[14] Federal Communications Commission, "Amendment of Parts 2 and 95 of the Commission's Rules to Establish a Medical Implant Communications Service (MICS) in the 402–405 MHz Band," *Report and Order*, FCC 03-32. Feb. 2003. Accessed: Jan. 14, 2026. [Online]. Available: https://docs.fcc.gov/public/attachments/FCC-03-32A1.pdf
[15] S. Gabriel, R. W. Lau, and C. Gabriel, "The dielectric properties of biological tissues: II. Measurements in the frequency range 10 Hz to 20 GHz," *Phys. Med. Biol.*, vol. 41, no. 11, pp. 2251–2269, 1996, doi: 10.1088/0031-9155/41/11/002. [Online]. Available: http://niremf.ifac.cnr.it/tissprop/
[16] M. T. Sebastian, R. Ubic, and H. Jantunen, "Low-loss dielectric ceramic materials and their properties," *Int. Mater. Rev.*, vol. 60, no. 7, pp. 392–412, 2015, doi: 10.1179/1743280415Y.0000000007.
[17] S. W. Ellingson, *Electromagnetics*, vol. 2. Blacksburg, VA, USA: Virginia Tech Publishing, 2020, pp. 33–35.
[18] IEEE Standard for Safety Levels With Respect to Human Exposure to Electric, "Magnetic, and Electromagnetic Fields," 3 kHz to 300 GHz, IEEE Std. C95.1-1991, 1999; IEEE Std. C95.1-2005, 2005; IEEE Std. C95.1-2019, 2019.
[19] "ICNIRP guidelines for limiting exposure to time varying electric field and magnetic field." Accessed: Nov. 14. 2025. [Online]. Available: https://www.icnirp.org/cms/upload/publications/ICNIRPLFgdl.pdf
[20] D. M. Pozar, "Microstrip antennas," *Proc. IEEE*, vol. 80, no. 1, pp. 79–91, Jan. 1992, doi: 10.1109/5.119568.
[21] C. A. Balanis, *Antenna Theory: Analysis and Design*, 4th ed. Hoboken, NJ, USA: Wiley, 2016.
[22] L.-J. Xu, Y.-X. Guo, and W. Wu, "Miniaturized circularly polarized loop antenna for biomedical applications," *IEEE Trans. Antennas Propag.*, vol. 63, no. 3, pp. 922–930, Mar. 2015, doi: 10.1109/TAP.2014.2387420.
[23] M. Fazeli, Y. Hong, W. Lee, and J. Park, "Implantable ferrite antenna for biomedical applications," *Microwave Opt. Technol. Lett.*, vol. 58, no. 11, pp. 2745–2749, 2016, doi: 10.1002/mop.30148.
[24] H. Li, Y. Guo, and S. Xiao, "Broadband circularly polarised implantable antenna for biomedical applications," *Electron. Lett.*, vol. 52, no. 7, pp. 504–506, 2016, doi: 10.1049/el.2015.4445.
[25] S. Xiao, C. Liu, Y. Li, X. M. Yang, and X. Liu, "Small-size dual-antenna implantable system for biotelemetry devices," *IEEE Antennas Wireless Propag. Lett.*, vol. 15, pp. 1723–1726, 2016, doi: 10.1109/LAWP.2016.2528987.
[26] B. Aslam, U. H. Khan, M. A. Azam, Y. Amin, J. Loo, and H. Tenhunen, "A compact implantable RFID tag antenna dedicated to wireless health care," *Int. J. RF Microw. Comput.-Aided Eng.*, vol. 27, no. 5, 2017, Art. no. e21094, doi: 10.1002/mmce.21094.
[27] R. Das and H. Yoo, "A wideband circularly polarized conformal endoscopic antenna system for high-speed data transfer," *IEEE Trans. Antennas Propag.*, vol. 65, no. 6, pp. 2816–2826, Jun. 2017, doi: 10.1109/TAP.2017.2694700.
[28] Z. Duan and L. Xu, "Dual-band implantable antenna with circular polarisation for ingestible capsule application," *Electron. Lett.*, vol. 53, no. 16, pp. 1090–1092, 2017, doi: 10.1049/el.2017.1681.
[29] M. W. A. Khan, E. Moradi, L. Sydänheimo, T. Björninen, Y. Rahmat-Samii, and L. Ukkonen, "Miniature coplanar implantable antenna on thin and flexible platform for fully wireless intracranial pressure monitoring system," *Int. J. Antennas Propag.*, vol. 2017, pp. 1–9, Jan. 2017.
[30] M. K. Magill, G. A. Conway, and W. G. Scanlon, "Tissue-independent implantable antenna for in-body communications at 2.36–2.5 GHz," *IEEE Trans. Antennas Propag.*, vol. 65, no. 9, pp. 4406–4417, Sep. 2017, doi: 10.1109/TAP.2017.2708119.
[31] L. Matekovits, J. Huang, I. Peter, and K. P. Esselle, "Mutual coupling reduction between implanted microstrip antennas on a cylindrical bio-metallic ground plane," *IEEE Access*, vol. 5, pp. 8804–8811, 2017, doi: 10.1109/ACCESS.2017.2703872.
[32] L. Matekovits, Y. Su, and I. Peter, "On the radiation mechanism of implanted antennas with large conformal ground plane," *IET Microw., Antennas Propag.*, vol. 11, no. 12, pp. 1765–1769, 2017, doi: 10.1049/iet-map.2017.0280.
[33] S. Bhattacharjee, S. Maity, S. R. Bhadra Chaudhuri, and M. Mitra, "Metamaterial-inspired wideband biocompatible antenna for implantable applications," *IET Microw., Antennas Propag.*, vol. 12, no. 11, pp. 1799–1805, 2018, doi: 10.1049/iet-map.2017.1143.
[34] J. Blauert, Y.-S. Kang, and A. Kiourti, "In Vivo testing of a miniature 2.4/4.8 GHz implantable antenna in postmortem human subject," *IEEE Antennas Wireless Propag. Lett.*, vol. 17, no. 12, pp. 2334–2338, Dec. 2018, doi: 10.1109/LAWP.2018.2874099.
[35] S. Das and D. Mitra, "A compact wideband flexible implantable slot antenna design with enhanced gain," *IEEE Trans. Antennas Propag.*, vol. 66, no. 8, pp. 4309–4314, Aug. 2018, doi: 10.1109/TAP.2018.2836463.
[36] R. Li, Y.-X. Guo, and G. Du, "A conformal circularly polarized antenna for wireless capsule endoscope systems," *IEEE Trans. Antennas Propag.*, vol. 66, no. 4, pp. 2119–2124, Apr. 2018, doi: 10.1109/TAP.2018.2804674.
[37] C. Liu, Y. Zhang, and X. Liu, "Circularly polarized implantable antenna for 915 MHz ISM-band far-field wireless power transmission," *IEEE Antennas Wireless Propag. Lett.*, vol. 17, no. 3, pp. 373–376, Mar. 2018, doi: 10.1109/LAWP.2018.2790418.
[38] S. A. A. Shah and H. Yoo, "Scalp-implantable antenna systems for intracranial pressure monitoring," *IEEE Trans. Antennas Propag.*, vol. 66, no. 4, pp. 2170–2173, Apr. 2018, doi: 10.1109/TAP.2018.2801346.
[39] Z.-J. Yang, L. Zhu, and S. Xiao, "Implantable circularly polarized patch antenna design for pacemaker monitoring based on quality factor analysis," *IEEE Trans. Antennas Propag.*, vol. 66, no. 10, pp. 5180–5192, Oct. 2018, doi: 10.1109/TAP.2018.2862242.
[40] K. Zhang et al., "A conformal differentially fed antenna for ingestible capsule system," *IEEE Trans. Antennas Propag.*, vol. 66, no. 4, pp. 1695–1703, Apr. 2018, doi: 10.1109/TAP.2018.2804673.
[41] Y. Zhang, C. Liu, X. Liu, K. Zhang, and X. Yang, "A wideband circularly polarized implantable antenna for 915 MHz ISM-band biotelemetry devices," *IEEE Antennas Wireless Propag. Lett.*, vol. 17, no. 8, pp. 1473–1477, Aug. 2018, doi: 10.1109/LAWP.2018.2849847.
[42] K. N. Ketavath, D. Gopi, and S. S. Rani, "In-vitro test of miniaturized CPW-fed implantable conformal patch antenna at ISM band," *IEEE Access*, vol. 7, pp. 43,547–43,554, 2019, doi: 10.1109/ACCESS.2019.2905661.
[43] G. Samanta and D. Mitra, "Dual-band circular polarized flexible implantable antenna using reactive impedance substrate," *IEEE Trans. Antennas Propag.*, vol. 67, no. 6, pp. 4218–4223, Jun. 2019, doi: 10.1109/TAP.2019.2905978.
[44] L. -J. Xu, Y. Bo, W. -J. Lu, L. Zhu, and C. -F. Guo, "Circularly polarized annular ring antenna with wide axial-ratio bandwidth," *IEEE Access*, vol. 7, pp. 59,999–60,009, 2019.
[45] Z.-J. Yang, L. Zhu, and S. Xiao, "Implantable wideband circularly polarized microstrip patch antenna via two pairs of degenerate modes," *IEEE Access*, vol. 7, pp. 4239–4247, 2019, doi: 10.1109/ACCESS.2018.2887234.
[46] K. Yeap, C. Voon, T. Hiraguri, and H. Nisar, "A compact dual-band implantable antenna for medical telemetry," *Microwave Opt. Technol. Lett.*, vol. 61, no. 9, pp. 2105–2109, 2019, doi: 10.1002/mop.31871.
[47] B. Biswas, A. Karmakar, and V. Chandra, "Miniaturised wideband ingestible antenna for wireless capsule endoscopy," *IET Microw., Antennas Propag.*, vol. 14, no. 4, pp. 293–301, 2020, doi: 10.1049/iet-map.2019.0439.
[48] Y. Fan, H. Liu, X. Liu, Y. Cao, Z. Li, and M. M. Tentzeris, "Novel coated differentially fed dual-band fractal antenna for implantable medical devices," *IET Microw., Antennas Propag.*, vol. 14, no. 2, pp. 199–208, 2020, doi: 10.1049/iet-map.2018.6171.
[49] S. Goswami and D. C. Karia, "A metamaterial-inspired circularly polarized antenna for implantable applications," *Eng. Rep.*, vol. 2, no. 10, 2020, Art. no. e12251, doi: 10.1002/eng2.12251.
[50] V. Kaim, B. K. Kanaujia, S. Kumar, H. C. Choi, K. W. Kim, and K. Rambabu, "Ultra-miniature circularly polarized CPW-fed implantable antenna," *Sci. Rep.*, vol. 10, Apr. 2020, Art. no. 6795.
[51] M. Usluer, B. Cetindere, and S. C. Basaran, "Compact implantable antenna design for MICS and ISM band biotelemetry applications," *Microwave Opt. Technol. Lett.*, vol. 62, no. 4, pp. 1581–1587, 2020, doi: 10.1002/mop.32185.
[52] A. Alshammari, M. Zada, A. Basir, A. Iqbal, and I. B. Mabrouk, "Compact in-band full-duplex antenna for deeply implantable biomedical IoT applications," *IEEE Internet Things J.*, vol. 13, no. 10, pp. 22,415–22,424, 2026, doi: 10.1109/JIOT.2026.3668723.
[53] S. M. A. Shah, M. Zada, O. Owais, A. Iqbal, and H. Yoo, "Miniaturized four-port MIMO implantable antenna for high-data-rate wireless-capsule-endoscopy applications," *IEEE Trans. Antennas Propag.*, vol. 71, no. 4, pp. 3123–3133, Apr. 2023, doi: 10.1109/TAP.2023.3243984.
[54] A. Lamkaddem, A. E. Yousfi, V. G. Posadas, and D. Segovia-Vargas, "Miniaturized dual band implantable antenna for implanted biomedical devices," *IEEE Access*, vol. 12, pp. 15,026–15,036, 2024, doi: 10.1109/ACCESS.2024.3357488.
[55] A. Lamkaddem, A. El Yousfi, Y. Huang, V. G. Posadas, and D. Segovia-Vargas, "Miniaturized wireless power transfer system with a dual-band implantable antenna for multifunctional

biomedical devices," *IEEE Sensors J.*, vol. 25, no. 16, pp. 31,473–31,488, Aug. 2025, doi: 10.1109/JSEN.2025.3587334.
[56] Q. -H. Wu, X. -W. Xuan, W. Wang, K. Li, and H. -B. Zhao, "Miniaturized implantable planar inverted-F antenna for 2.45 GHz biotelemetry," *Microwave Opt. Technol. Lett.*, vol. 62, no. 1, pp. 391–396, 2020.
[57] Y. Zhang, C. Liu, X. Liu, and K. Zhang, "A miniaturized circularly polarized implantable RFID antenna for biomedical applications," *Int. J. RF Microw. Comput.-Aided Eng.*, vol. 30, no. 3, pp. e22105, 2020, doi: 10.1002/mmce.22105.
[58] V. Kaim, B. K. Kanaujia, and K. Rambabu, "Quadrilateral spatial diversity CP MIMO cubic implantable antenna system," *IEEE Trans. Antennas Propag.*, vol. 69, no. 3, pp. 1260–1272, Mar. 2021, doi: 10.1109/TAP.2020.3016483.
[59] J. Lai et al., "Dual-polarized omnidirectional DRA for capsule endoscopy," *IEEE Access*, vol. 9, pp. 14,779–14,786, 2021, doi: 10.1109/ACCESS.2021.3052601.
[60] W. Cui et al., "Design of circularly polarized implantable antenna for wireless intracranial pressure monitoring system," *Int. J. RF Microw. Comput.-Aided Eng*, vol. 32, no. 4, pp. e23053, 2022, doi:10.1002/mmce.23053
[61] Y. Feng et al., "Compact miniaturized implantable antenna for ISM-band cardiac pacemakers," *Sci. Rep.*, vol. 12, 2022, Art. no. 238.
[62] A. Iqbal, P. R. Sura, M. Al-Hasan, I. B. Mabrouk, and T. A. Denidni, "Wireless power transfer system for deep-implanted biomedical devices," *Sci. Rep.*, vol. 12, no. 1, 2022, Art. no. 13689, doi: 10.1038/s41598-022-18000-6.
[63] V. Kaim, B. K. Kanaujia, S. Kumar, H. C. Choi, K. W. Kim, and K. Rambabu, "Electrically small CP UWB intraocular antenna system for retinal prosthesis," *IEEE Trans. Biomed. Eng.*, vol. 69, no. 11, pp. 3504–3515, Nov. 2022, doi: 10.1109/TBME.2022.3171842.
[64] D. Sharma et al., "Compact dual-band conformal antenna for leadless cardiac pacemakers," *Sci. Rep*, vol. 12, 2022, Art. no. 3165.
[65] C. Xiao, S. Hao, and Y. Zhang, "915 MHz miniaturized loop conformal antenna for capsule endoscope," *IEEE Trans. Antennas Propag.*, vol. 70, no. 11, pp. 10,233–10,244, Nov. 2022, doi: 10.1109/TAP.2022.3197272.
[66] Y. E. Yamac, M. Ciflik, and S. C. Basaran, "Miniaturized multiband implantable antenna designs," *Int. J. RF Microw. Comput.-Aided Eng*, vol. 32, no. 11, pp. 1–12, 2022, doi: 10.1002/mmce.23335.
[67] S. Ahlawat, B. K. Kanaujia, K. Rambabu, I. Peter, and L. Matekovits, "Circularly polarized differential intra-oral antenna for tongue drive system," *Sci. Rep*, vol. 13, Jun. 2023, Art. no. 9935.
[68] D. Jing, H. Li, X. Ding, W. Shao, and S. Xiao, "Compact and broadband circularly polarized implantable antenna," *IEEE Antennas Wireless Propag. Lett.*, vol. 22, no. 6, pp. 1236–1240, Jun. 2023, doi: 10.1109/LAWP.2023.3237558.
[69] V. Kaim, N. Singh, B. K. Kanaujia, L. Matekovits, K. P. Esselle, and K. Rambabu, "Multi-channel implantable cubic rectenna MIMO system with CP diversity in orthogonal space for enhanced wireless power transfer in biotelemetry," *IEEE Trans. Antennas Propag.*, vol. 71, no. 1, pp. 200–214, Jan. 2023, doi: 10.1109/TAP.2022.3222695.
[70] D. Sharma, B. K. Kanaujia, S. Kumar, K. Rambabu, and L. Matekovits, "Low-loss MIMO antenna wireless communication system for 5G cardiac pacemakers," *Sci. Rep.*, vol. 13, no. 1, pp. 9557, Jun. 2023, doi: 10.1038/s41598-023-36209-x.
[71] J. Zhang et al., "Compact dual-band implantable antenna for arteriovenous grafts," *IEEE Trans. Antennas Propag.*, vol. 71, no. 6, pp. 4759–4771, Jun. 2023.
[72] Z. Song, X. Zheng, Y. Shi, and Y. Wang, "Implantable small ultra-wideband circularly polarized antenna for continuous blood pressure monitoring," *Sci. Rep.*, vol. 14, no. 1, pp. 25199, 2024, doi: 10.1038/s41598-024-74512-3.
[73] A. A. Chandran, M. Kanagasabai, S. Subbaraj, and M. G. N. Alsath, "Miniaturized circularly polarized implantable antenna for biotelemetry applications," *IEEE Antennas Wireless Propag. Lett.*, vol. 24, no. 12, pp. 4535–4539, Dec. 2025, doi: 10.1109/LAWP.2025.3599695.
[74] J. Chu et al., "An ultrawideband implantable antenna with hybrid polarization for human health monitoring," *IEEE Antennas Wireless Propag. Lett.*, vol. 24, no. 9, pp. 2859–2863, Sep. 2025, doi: 10.1109/LAWP.2025.3575448.
[75] A. Essa, E. Almajali, F. Barneih, J. Yousaf, R. E. Amaya, and S. Mahmoud, "A compact tissue-insensitive ultra-wideband implantable antenna for wireless power transfer in implantable medical devices," *IEEE Open J. Antennas Propag.*, vol. 6, no. 6, pp. 1989–2006, Dec. 2025, doi: 10.1109/OJAP.2025.3611662.
[76] L. Harlan, M. Susila, S. Kumar, H. C. Choi, and K. W. Kim, "Reconfigurable ultra-miniaturized MIMO antenna for tissue-independent communication in injectable medical implants," *IEEE Access*, vol. 13, pp. 22,663–22,677, 2025, doi: 10.1109/ACCESS.2025.3535780.
[77] Y. A. Kamel, H. A. Mohamed, H. ELsadek, and H. M. ELhennawy, "RF communication between dual band implantable and on body antennas for biotelemetry application," *Sci. Rep.*, vol. 15, no. 1, Feb. 2025, Art. no. 4065, doi: 10.1038/s41598-025-86235-0.
[78] S. Kumaravel and M. Karthikeyan, "Circularly polarized dual-band resonance in a miniaturized implantable antenna using combined hexagonal and rhombic patches," *Sci. Rep*, vol. 15, no. 1, Jan. 2025, Art. no. 3543, doi: 10.1038/s41598-025-86882-3.
[79] J. Shang, S. Gao, Y. Yu, and Z. Wang, "Miniaturized broadband antenna for implantable biomedical devices," *Microwave Opt. Technol. Lett*, vol. 67, no. 8, Aug. 2025, Art. no. e70333.
[80] L.-J. Xu, Z. Zhou, M. Liang, M. Huang, and Q. Liu, "Circularly polarized implantable antenna in hemisphere cap for deeply embedded blood glucose monitoring applications," *Microwave Opt. Technol. Lett.*, vol. 67, no. 8, Aug. 2025, Art. no. e70338.
[81] Y. Chen, X. Xuan, M. Li, D. Jiang, and H. Li, "Implantable antenna immunosensor based on Au-decorated graphene film for wireless CEA detection," *Sens. Actuators, B*, vol. 416, Oct. 2024, Art. no. 136037, doi: 10.1016/j.snb.2024.136037.
[82] L. Matekovits, F. Mir, G. Dassano, and I. Peter, "Deeply implanted conformal antenna for real-time bio-telemetry applications," *Sensors*, vol. 24, no. 4, Feb. 2024, Art. no. 1170, doi: 10.3390/s24041170.
[83] I. Peter, G. Strnad, A.-B. Kacsó, and R. Spotorno, "Characterization of anodized Ti-based alloys: Wettability, corrosion resistance, and biomechanical performance," *IEEE Access*, vol. 13, pp. 213,508–213,522, 2025, doi: 10.1109/ACCESS.2025.3645698.
[84] G. Strnad, L. Jakab-Farkas, F. S. Gobber, and I. Peter, "Synthesis and characterization of nanostructured oxide layers on Ti–Nb–Zr–Ta and Ti–Nb–Zr–Fe biomedical alloys," *J. Functional Biomaterials*, vol. 14, no. 4, Mar. 2023, Art. no. 180, doi: 10.3390/jfb14040180.
[85] A.-B. Kacsó and I. Peter, "A review of past research and some future perspectives regarding titanium alloys in biomedical applications," *J. Functional Biomaterials*, vol. 16, no. 4, pp. 144, Apr. 2025, doi: 10.3390/jfb16040144.
[86] A.-B. Kacsó, L. Matekovits, and I. Peter, "Titanium alloys at the interface of electronics and biomedicine: A review of functional properties and applications," *Electron. Mater.*, vol. 7, no. 1, 2026, Art. no. 1, doi: 10.3390/electronicmat7010001.
[87] M. P. Ferraz, "Bone grafts in dental medicine: An overview of autografts, allografts and synthetic materials," *Materials*, vol. 16, no. 11, 2023, Art. no. 4117, doi: 10.3390/ma16114117.
[88] E. Marin and A. Lanzutti, "Biomedical applications of titanium alloys: A comprehensive review," *Materials*, vol. 17, no. 1, 2023, Art. no. 114, doi: 10.3390/ma17010114.
[89] I. Peter, "Investigations into Ti-based metallic alloys for biomedical purposes," *Metals*, vol. 11, no. 10, 2021, Art. no. 1626, doi: 10.3390/met11101626.
[90] N. C. Paxton, M. C. Allenby, P. M. Lewis, and M. A. Woodruff, "Biomedical applications of polyethylene," *Eur. Polym. J.*, vol. 118, pp. 412–428, 2019, doi: 10.1016/j.eurpolymj.2019.05.037.
[91] N. S. Arul and V. D. Nithya, Eds., *Revolution of Perovskite: Synthesis, Properties and Applications Materials Horizons: From Nature to Nanomaterials*. Singapore: Springer-Verlage, 2020.
[92] R. E. Ashtiani et al., "The role of biomaterials and biocompatible materials in implant-supported dental prosthesis," *Evidence-Based Complementary Alternative Med.*, vol. 2021, pp. 1–9, Aug. 2021, doi: 10.1155/2021/3349433.
[93] A. J. T. Teo, A. Mishra, I. Park, Y.-J. Kim, W.-T. Park, and Y.-J. Yoon, "Polymeric biomaterials for medical implants and devices," *ACS Biomater. Sci. Eng.*, vol. 2, no. 4, pp. 454–472, 2016, doi: 10.1021/acsbiomaterials.5b00429.
[94] T. Safronova, V. I. Putlayev, A. G. Veresov, A. V. Kuznetsov, M. A. Shekhirev, and K. A. Agahi, "Biocompatible ceramics for implants based on calcium phosphates," *MRS Proc.*, vol. 951, 2006, Art. no. 0951-E12-31, doi: 10.1557/PROC-0951-E12-31.
[95] M. Alizadeh-Osgouei, Y. Li, and C. Wen, "A comprehensive review of biodegradable synthetic polymer-ceramic composites and their manufacture for biomedical applications," *Bioactive Mater.*, vol. 4, pp. 22–36, Dec. 2019, doi: 10.1016/j.bioactmat.2018.11.003.
[96] M. F. Maitz, "Applications of synthetic polymers in clinical medicine," *Biosurface Biotribol.*, vol. 1, no. 3, pp. 161–176, 2015, doi: 10.1016/j.bsbt.2015.08.002.
[97] Y.-W. Chen, J. Moussi, J. L. Drury, and J. C. Wataha, "Zirconia in biomedical applications," *Expert Rev. Med. Devices*, vol. 13, no. 10, pp. 945–963, 2016, doi: 10.1080/17434440.2016.1230017.
[98] H. Seitz, S. Marlovits, I. Schwendenwein, E. Müller, and V. Vécsei, "Biocompatibility of polyethylene terephthalate (Trevira® hochfest) augmentation device in repair of the anterior cruciate ligament," *Biomaterials*, vol. 19, nos. 1–3, pp. 189–196, 1998, doi: 10.1016/S0142-9612(97)00201-9.

Open Access funding provided by 'Politecnico di Torino' within the CRUI CARE Agreement